Received —; | Revised —; | Accepted —

DOI: xxx/xxxx

ARTICLE TYPE

Vorogrid: a static-aware variable-density Voronoi mesh to design the tube structure tessellation of tall buildings

Francesco Laccone*[1] | Domenico Gaudioso[2] | Luigi Malomo[1] | Paolo Cignoni[1] | Maurizio Froli[2]

[1]ISTI, CNR, Italy
[2]Department of Civil and Industrial Engineering, University of Pisa, Italy

***Correspondence**
Francesco Laccone, ISTI, CNR, Via Moruzzi 1, 56124 Pisa, Italy. Email: francesco.laccone@isti.cnr.it

Summary

In the context of tall building design, the tube concept represents one of the most performing systems. The diagrid is the widespread type of tube system and consists of a diagonal grid of beams that wraps the building, forming a diamond pattern. It performs as lateral bracing and is additionally able to sustain vertical loading through axial forces. Despite its efficiency, a growing interest is recently observed in alternative geometries to replace the diagrid pattern and improve the architectural impact conferred by the building skin aesthetics on the urban environment. The paper pursues the use of a Voronoi mesh, in which the geometry of the cells is steered to known schemes for the structural design of a cantilever tube structure. The objective is to mimic a macroscopic structural behavior through a topology and size modification of the Voronoi mesh that increases the density for creating resisting paths with higher stiffness. The paper proposes a novel method Vorogrid for designing a new class of tall buildings equipped with an organic-looking and mechanically-sound tube structure, which makes them a valuable alternative to competitors (diagrid, hexagrid, random Voronoi). Diagrids and hexagrids still remain more efficient in terms of forces and displacements but are characterized by a more usual appearance, instead Vorogrid offers more design control and better performances on average with respect to random Voronoi structures. This method is streamed into a pipeline that includes grid initialization strategies, geometric and structural optimization to mitigate the effects of the grid randomness, and structural sizing.

KEYWORDS:
tall buildings, mesh, steel structure, structural optimization, cantilever, diagrid, hexagrid, algorithm

1 | INTRODUCTION

Modern tall buildings are characterized by a large-scale impact on the urban context and the natural resources their construction and management need. In the design phase, primary attention is devoted to the global geometry for the building identity as a signature in the skyline. Then, in a later stage, the design is oriented on building/structural performances and material resources optimization. For a given global geometry, the external surfaces and specifically their façade patterns have a prominent role. They are usually the areas where different and sometimes even opposite performance requirements are synthesized. Furthermore, the designer's task is to find a good compromise. For tall buildings, it is common to have load-bearing members on the external surfaces. Thus, apart from characterizing the façade aesthetics, they can guarantee the flow of forces.

The structural design is mostly pushed by the requirements of efficiency and sustainability, and by the increasing

heights these buildings tend to. Concurrently, lateral loads given by wind and earthquakes become more critical. These factors have brought innovation and development of several structural systems (Gunel & Ilgin, 2007), such as the tube structure (Sarcheshmehpour & Estekanchi, 2021), outriggers (Kim, Lim, & Lee, 2020), the tube-in-tube (Sarcheshmehpour, Estekanchi, & Moosavian, 2020), the bundled towers (Laccone, Casali, Sodano, & Froli, 2021), the megaframes Zhou, Qian, Huang, & Yao (2021), to fulfil strength and stiffness demands.

Among them, the tube is a widespread structural solution. One of its derivations is the diagrid system (Moon, Connor, & Fernandez, 2007), in which a grid of diamond cells replaces the surface of the tube, hence the name. The edges of this pattern can span single or multiple floors, but globally they perform as a diffuse bracing system loaded through axial forces. From a mechanical perspective, this system is efficient (Asadi & Adeli, 2017) and robust (C. Liu & Fang, 2020) and is being successfully employed since about 20 years ago, becoming a standard structural scheme.

Given the iconic impact that a tall building possesses from an architectural point of view, current research questions are: (i) whether a family of alternative patterns exists to fulfill both the need to have a different and recognizable aesthetic appearance and to have load-bearing capacity as a discrete tube structure; (ii) how it can be designed. In tall building practice, confirming this trend, some unconventional tube patterns started appearing (e.g., the O-14 Skyscraper in Dubai, United Arab Emirates, 2010).

This paper introduces a methodology entitled *Vorogrid* for generating an alternative family of polygonal patterns that serve as tube structures. This methodology aims to generate different Voronoi patterns that mimic typical structural schemes occurring in tall buildings or generally in cantilever tubes by altering the density of the seeds. The main idea is to hide specific structural strategies fostering the flow of forces in a discrete system made of organic and pleasant-looking patterns.

Current state-of-the-art methods adopt Voronoi tessellations (Angelucci & Mollaioli, 2018; Mele, Fraldi, Montuori, Perrella, et al., 2019) that are derived from hexagonal honeycomb systems, the closest tessellation having a regular distribution of seeds. The seeds of this regular pattern are then perturbed by using three parameters, the random angle, the random scale factor, and the irregularity factor, which become the descriptors of the tessellation. Conversely, in the present case, the distribution of seeds is not regular and they are moved to increase the density of Voronoi cells in specific areas where a higher mesh stiffness is desired. Thus, better performances and more control in design are achieved.

In the following, after a brief outline of the research context for tall building design and optimization, for diagrids and poly-grids (pointing to the grid of cells with a generic polygonal shape) and some hints on the use of Voronoi meshes in design, the methodology of the present work is proposed. This methodology is shown in fig. 1 and has been implemented on a regular tall building model akin to the Sinosteel International Plaza building. Different pattern solutions are generated, and geometric and structural optimization alternatives are presented to enhance the grid's quality. Finally, the selected case studies are discussed and compared to other state-of-the-art solutions.

2 | RELATED WORK

Tall building design and optimization

A key role in the performance of tall buildings is played by the conceptual design of the structure, which can be tackled at different and inter-related levels, as well described in Tomei, Imbimbo, & Mele (2018): at the global level, for designing the shape and establishing a specific macroscopic behavior; at the intermediate level, for defining the organization of the elements, their relationships, and fulfill local stiffness/strength demands; at the detail level. The present work is focused on the intermediate-level conceptual design of tube structure tessellations.

Due to the problem complexity and the high number of variables involved, the design phase is usually supported by computational tools and by optimization routines. Indeed, because of the object size, even small adjustments produce a large-scale effect on the required resources and costs. However, optimizing a tall building is a large-scale problem and is intense from the computational viewpoint. Thus, the choice of the optimization approach and the appropriate design variables is fundamental (Aldwaik & Adeli, 2014). Within this framework, Adeli and colleagues introduced pioneering methods such as the neural dynamics models (Adeli & Park, 1995 1998) and parallel computing methods (Adeli & Cheng, 1994; Adeli & Kumar, 1995). These are important milestones and have been used to solve several engineering problems, such as the cost optimization of large space steel structures (Sarma & Adeli, 2001 2003), the shape and topology optimization of free-form roofs (Kociecki & Adeli, 2014 2015), the vibration control of base-isolated irregular buildings (Gutierrez Soto & Adeli, 2017). Alternative methods incorporate game theory in the design optimization (Mahjoubi & Bao, 2021), neural networks (Li, Snaiki, & Wu, 2021; Oh, Glisic, Kim, & Park, 2019) and

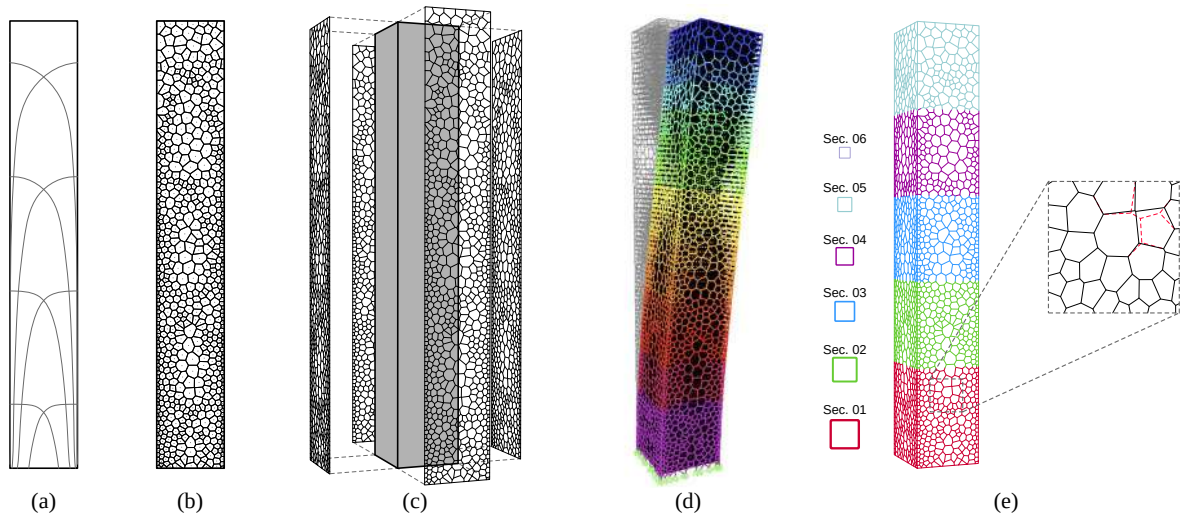

FIGURE 1 Vorogrid pipeline for generating variable-density Voronoi tube structures: (a) structural scheme; (b) seeds population and Voronoi mesh; (c) building of a 3D model; (d) structural analysis; (e) optimization and cross-section refinement.

topology optimization algorithms (Angelucci, Spence, & Mollaioli, 2020; Beghini, Beghini, Katz, Baker, & Paulino, 2014; Lee & Tovar, 2014).

From diagrids to poly-grids

The design and optimization of diagrids is a particularly fertile research area. The diagonal columns and the ring beams create a triangular tessellation, which is simple to model and generally applicable since any form can be discretized into triangular sub-modules. Other benefits are related to the structural behavior: both vertical and lateral loads cause prevalent axial internal stress; shear lag effects and racking deformations are usually low (Lacidogna, Scaramozzino, & Carpinteri, 2019; C. Liu, Li, Lu, & Wu, 2018).

The simplicity of altering the triangular mesh has paved the way for several studies aiming at finding the best design. Moon (2008) firstly investigated the diagrid members' inclination in relation with the building height and aspect ratio, looking at the best material utilization rate. Montuori, Mele, Brandonisio, & De Luca (2014) analyzed stiffness vs strength design of patterns. Zhao & Zhang (2015) proposed optimal geometries for curved and varying-angles straight diagonals under wind and seismic loads. Asadi & Adeli (2018) investigate the performance of steel diagrid structures with different building heights and aspect ratios to evaluate their key seismic performance factors. Tomei et al. (2018) included the cross-section sizing in a more complex optimization method that also considers non-uniform patterns, which can not be simplified into reduced models. Similarly, Angelucci & Mollaioli (2017) proposed a strength optimization method for stiffness-designed patterns.

The design of polygonal patterns as tall building tube structures is a recent trend in research. The hexagrid system was firstly introduced in Mashhadiali & Kheyroddin (2013) in replacement of diagrids to improve the architectural appearance of the façade, to increase daylight, to reduce the amount of steel and the building mass, and to provide ductility. Evidently, reducing the node connectivity from triangle- to poly-mesh has a great effect on the node in terms of bearing capacity, fabrication, and costs, but, most importantly, it makes the grid a bending-dominated structure. Thus, the efficiency of hexagrid has been the main research question of Montuori, Fadda, Perrella, & Mele (2015), which additionally provided a stiffness design criterion and a generalized homogenization approach for tall buildings' structural patterns based on beam analogy (representative volume element, RVE). An alternative conceptual design tool has been provided by Bruggi (2020), in which the box grid is modeled as a shell and the set of lattice is assigned through a multi-material topology optimization.

To enable more design freedom through nature-inspired patterns, Angelucci & Mollaioli (2018) proposed a procedure for generating Voronoi-like patterns by perturbing a regular honeycomb configuration. The Voronoi mesh is consistently applied in the work of Mele et al. (2019), where the RVE approach has been extended on a statistical basis to take into account the inherent irregularity, non-periodicity, and randomness of the grid.

Voronoi mesh as a design tool

The Voronoi tessellation is a partition of a surface into cells, whose property is to be close to each of a given set of points, called vertices or seeds. Although Voronoi meshes can be

found in literature across multiple research areas, from computer graphics to finite element approaches, more recently they are appreciated and increasingly adopted into digital fabrication. Cucinotta, Raffaele, & Salmeri (2019) introduced a stress-based topology optimization method for digitally manufactured objects. Fantini & Curto (2018); B. Liu, Cao, Zhang, Jiang, & Lu (2021) deliver volumetric porous structures. Martínez, Dumas, & Lefebvre (2016); Martínez, Hornus, Song, & Lefebvre (2018) introduce parametric strategies for producing general additive-manufactured objects. Indeed, Voronoi meshes are characterized by low node connectivity equal to 3 and an inherent organic-looking visual lightness.

Inspired by lightweight and robust lattice structures that appear in nature, some works addressed the use of a Voronoi mesh for structural purposes at a larger scale. The works Froli & Laccone (2017); Pietroni et al. (2015); Tonelli et al. (2016) proposed and validated a method for generating a Voronoi mesh, whose cells conform to the principal stress directions of the underlying surface, and are scaled and stretched accordingly. Su, Wu, Ji, & Sun (2020) developed a morphogenesis method for Voronoi structures of high architectural and structural performances. A design-to-manufacture pipeline is proposed by Hua, Hovestadt, & Tang (2020) to handle timber Voronoi shells delivery.

3 | VOROGRID FRAMEWORK

The methodology proposed in the current work to generate the Voronoi mesh and use it as tube structural grid is depicted in fig. 1 and is described in the following steps. It constitutes a design tool whose end goal is tuning the geometry of a Voronoi pattern to comply with a desired structural behavior. The first step is the selection of plausible static schemes for the tube structure (fig. 1 a), which can be of any nature, i.e. experience-based, derived by hand calculations or numerical computations. These schemes highlight curves and surfaces on the tube that become candidate paths or areas to drive the tessellation. Then, a variable density Voronoi tessellation is defined, in which the Voronoi seeds are attracted by the highlighted paths or areas to form denser regions (fig. 1 b). More formally, the distance metric varies along the surface such that near the attractors, the distance is less weighted. Therefore the Voronoi tessellation becomes denser approaching those regions. The cross-section of the grid elements is initialized according to the stiffness-based procedure in Mele et al. (2019).

A structural model is assembled to perform finite element analyses under lateral and vertical loads (fig. 1 d). In this setting, unlike diagrids, polygonal cells result in bending-stressed elements. A generic cell may exhibit high stress because of its size, orientation and position with respect to neighboring elements, i.e. other cells or slabs. Therefore, an optimization is carried out to globally improve the static performances of the structure by perturbing the Voronoi centroids. Finally, appropriate members' cross-sections are chosen by assigning commercial section properties to clusters of Vorogrid's beams (i.e. obtained by segmenting the tube into stacking modules throughout the height) (fig. 1 e).

4 | IMPLEMENTATION

The proposed methodology is applied to a tall building model with a square floor plan to reduce the number of variables and avoid shape-variation-related phenomena. The tube is therefore made of four all-equal rectangular surfaces.

All steps are streamed in the Rhinoceros-grasshopper environment McNeel & Associates (2020). For the structural analysis, Karamba3D Preisinger & Heimrath (2014) has been used for a direct feedback of the parametric model and within the optimization routine, while SAP2000 Computers and Structures, Inc. (2021) has been employed to carry out the final 3D models.

Fig. 2 reports the structural schemes considered as seeds' attractors (areas or lines), namely:

(a) outriggers and belt truss scheme;
(b) megacolums;
(c) central shear wall and outriggers;
(d) megaframe;
(e) braced tube (Moon, 2010);
(f) principal stress lines on a uniformly-loaded equivalent cantilever (Cascone, Faiella, Tomei, & Mele, 2021).

The symmetry of the building about the plan diagonals lowers the problem complexity and, as a consequence, allows generating the grid on a single building face for computation efficiency. Thus, the adopted schemes are 2D, and the Voronoi diagram is geometrically defined and optimized on a single face. Later, the obtained Voronoi face is mapped in 3D by replicating and rotating it by 90° about the building corner. Remarkably, this mapping produces Vorogrids mirrored with respect to the building corner, so their beams meet at the same nodes. The 3D model is employed to solve the sizing problem and to verify the design solution.

4.1 | Model configuration, materials and loads

The building model adopted for the design applications is equivalent to the model considered in the work by Montuori et

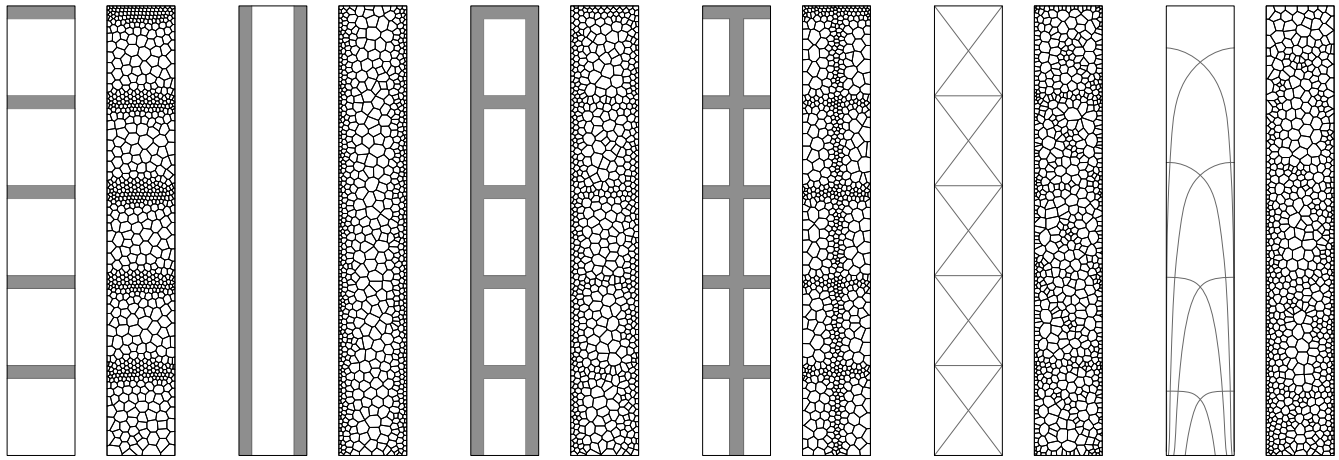

FIGURE 2 Structural schemes (areas and lines) adopted in this work to attract Voronoi seeds, and their relative Vorogrid, from left to right: a) outrigger and belt truss; b) megacolumns; c) megaframe; d) central shear wall and outriggers; e) braced tube; f) cantilever stress lines. The width of the area regions adopted in the following experiments is 10 m; the Voronoi mesh is obtained with the technique remeshing-from-distance (sec. 4.2).

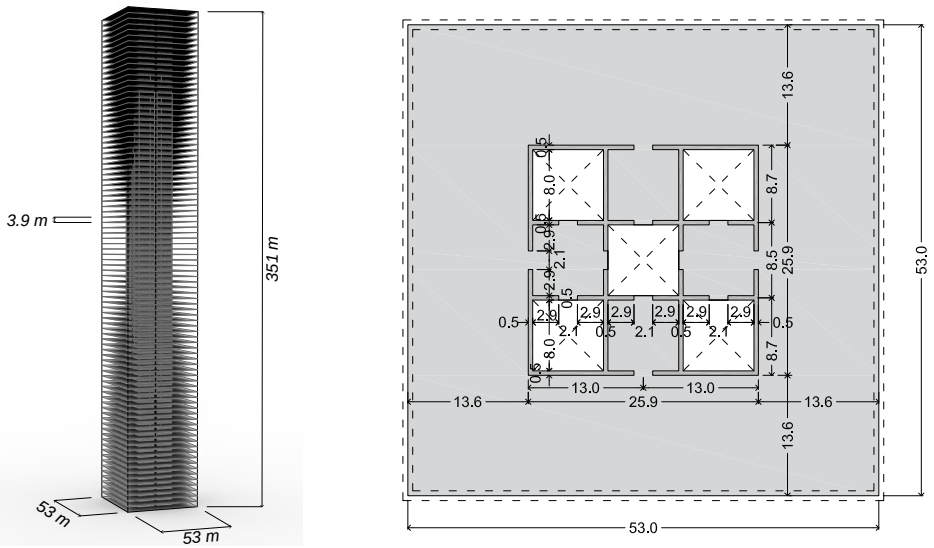

FIGURE 3 The building model adopted in this work and schematic plan view.

al. (2015), namely the Sinosteel International Plaza tall building. This 90 stories building has a square section of dimension $53x53$ m, height $H = 351$ m, and interstory height $h = 3.9$ m (fig. 3).

Apart from the external tube structure that constitutes the design domain of this work, the building has another vertical structure, i.e. a central concrete core organized as in fig. 3 that provides vertical and lateral resistance. This core has a constant cross-section throughout the height; its walls are 0.5 m thick made of C45/55 concrete ($E_c = 36.28$ GPa, $f_{ck} = 45$ MPa). The grid elements are made of S275 steel ($E_s = 210$ GPa, $f_{yk} = 275$ MPa).

The building is loaded by dead loads given by the own weight of the structural elements G_1, automatically deduced from the cross-section properties. The slabs bear a load of $G_1 + G_2 = 7$ kN/m^2, summing the contribution of structural an non-structural weights, and a live load of $Q_k = 3$ kN/m^2. Horizontally, a uniform load wind action of $Q_w = 200$ kN/m along the building height is considered. These are later combined using the Eurocode (EC) load combination schemes at

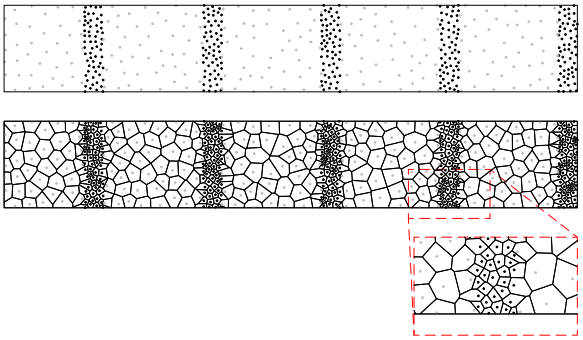

FIGURE 4 Voronoi diagram with area attractors derived from a random distribution of seeds with different densities, case (a) (sec. 4).

the Ultimate Limit State (ULS) and at Serviceability Limit State (SLS). The outer tube is supposed to be anchored on the slabs to benefit from the rigid diaphragm effect, also identified in Montuori et al. (2015), and from the coupling with the core.

4.2 | Seeds population

Given a set of n points called seeds in the Euclidean plane, each point P_i for $i = 1, .., n$ can be connected with its neighboring ones to form a triangular mesh. The Voronoi diagram is defined as the partitioning of the plane into convex regions which contain the portion of the plane closest to each seed; Voronoi diagram is known to be dual or reciprocal of the Delaunay triangulation of the seeds, e.g. the Delaunay triangulation can be derived by just connecting the dots that correspond to Voronoi regions that are adjacent. Similarly, the vertexes of an existing triangulations can be used as seeds for generating a Voronoi Diagram. When seeds are well distributed Voronoi diagrams usually produce cells that tend to be regular polygons, or tend to irregular shapes contrarily. In any case, the density and the shape of the cell is totally dependent on the number and position of the seeds. In the present work, several strategies are explored for seed placement that lead to the creation of a Voronoi diagram with some desired properties. These strategies can be grouped based on whether the seeds are initialized as a regular or a random population. When dealing with areas, implementing a random Voronoi is straightforward: the tube surface can be differentiated into two areas where random seeds are distributed with different densities (fig. 4). Obtaining a regular seeds distribution with this strategy is still possible but produces irregular polygons on the adjacency between areas with different densities. Therefore, a smoother transition can be produced using a remesh-from-distance procedure. The starting point is a regular quad mesh, whose vertices are colored based on the distance from the area attractors. Then, an isotropic remeshing is performed through

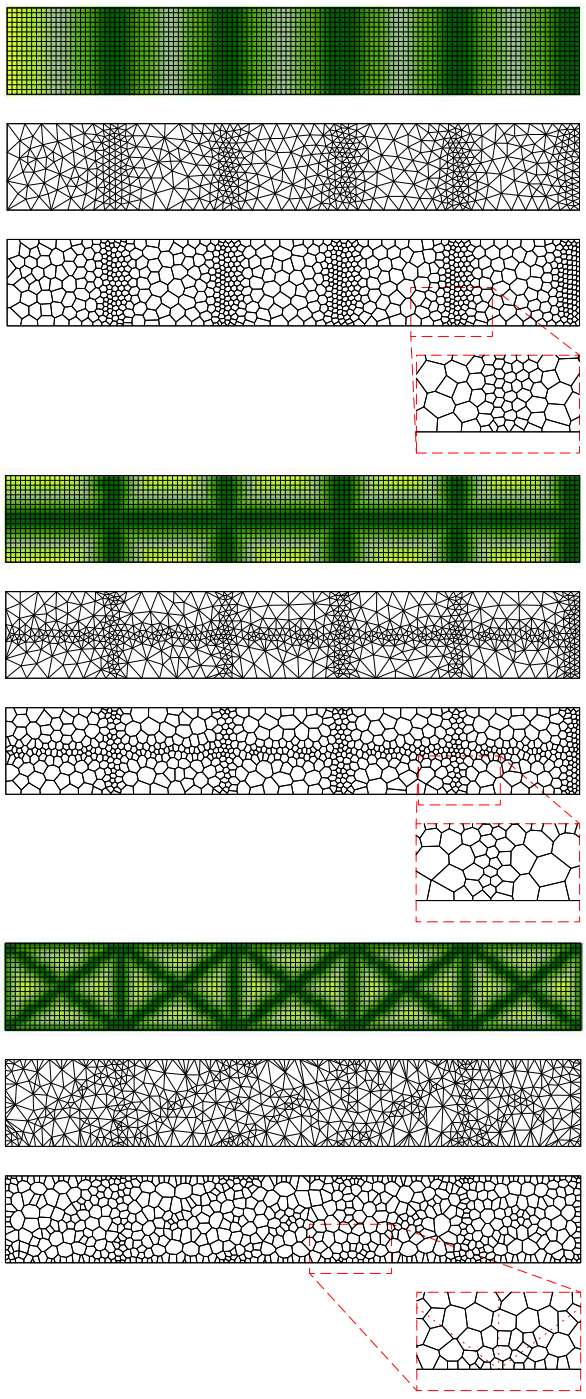

FIGURE 5 Voronoi diagram with areas and lines attractors derived from remeshing-from-distance and dualization procedure, cases (a), (d) and (e) (sec. 4): from top quad mesh (the vertex color stands for the distance to the area attractor, the closer the darker), remesh-by-color Delaunay triangulation, dual Voronoi mesh.

RemeshByColor (Piker, 2013) that creates a Delaunay triangulation. With reference to fig. 5 , the Voronoi mesh is

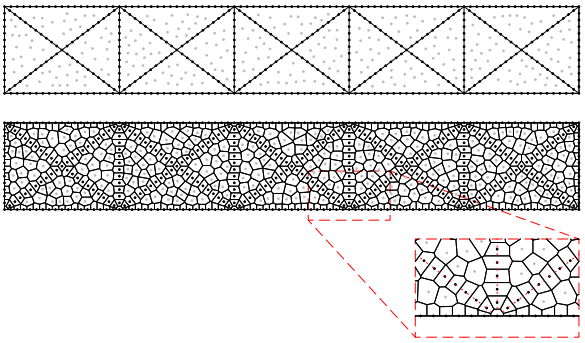

FIGURE 6 Voronoi diagram with equally-spaced seeds on the line attractors and random distribution of seeds elsewhere, case (e) (sec. 4).

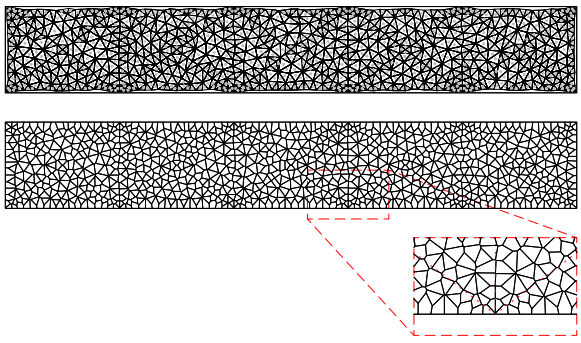

FIGURE 7 Voronoi diagram obtained from the barycenters of the dual triangle mesh (computed from fig. 6), case (e) (sec. 4).

obtained simply by dualization. This method can also be suitably applied to line paths (fig. 5 , bottom) by computing the distance from the line attractors.

Instead, when dealing with line constraints, it is harder to find a random population of seeds that generates a Voronoi diagram that includes such lines. The simple solution of placing (equally- or randomly-spaced) seeds along with the line attractors and populating the remaining part of the surface randomly (fig. 6) has the drawback of creating a series of voids centered on the line attractors. This configuration implies that the load-bearing material, which is expected to be aligned with the lines, is randomly oriented due to the randomness of the neighboring seeds (fig. 6 , closeup). To overcome this problem, two strategies are proposed. The first is to obtain a new Voronoi mesh using as seeds barycenters of the dual triangulation of the Voronoi diagram obtained by the simple approach (fig. 7). The second solution is to place the seeds symmetrically on offset curves of the attractors' lines. Thus, the generated Voronoi edges will fall along the attractor lines and be aligned to them (fig. 8). These two strategies produce irregular cells and small edges in which peak stress and consequently plasticity can concentrate. As shown in sec. 4.4, this issue can be partially solved by improving the mesh quality. However, due to its consistency and better resulting quality, the strategy of remeshing-from-distance is adopted in the Vorogrid pipeline.

4.3 | Stiffness-based preliminary design

Following the remeshing-from-distance grid initialization, a tentative cross-section is required to convert the Voronoi edges into beams and run structural simulations in the further steps of the Vorogrid method. For this purpose, Mele et al. (2019) approach is adopted. Hence, the entire tube structure, i.e. the design space adopted in this work, is homogenized as a large

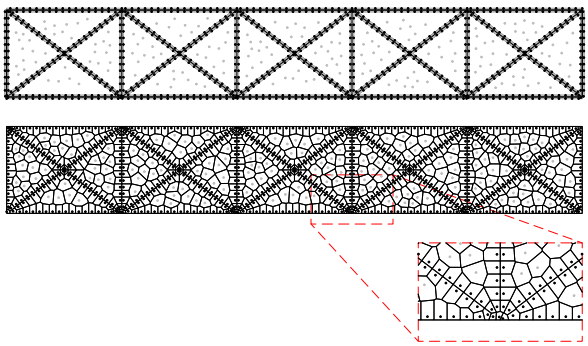

FIGURE 8 Voronoi diagrams with equally-spaced seeds on offset lines of the attractors and random distribution of seeds elsewhere, case (e) (sec. 4).

cantilever beam with a hollow cross-section, whose mechanical properties account for the topology and size of the grid. The grid topology and size can be inversely tuned by targeting the limit deflection of the homogenized cantilever. The design criterion is stiffness-based.

The problem of Voronoi meshes is the non-regular topology and non-uniform distribution of structural material, which do not allow to identify of a periodic unit cell, namely a Representative Volume Element (RVE). Consequently, Mele et al. (2019) observed a correlation between irregular grids and periodic hexagrids that can be expressed through correction factors on a statistical basis. Thus, by knowing the irregularity degree of the grid $\alpha \in [0, 1]$ and the relative density ρ, the averaging mechanical properties of the grid members can be found. The irregularity degree is $\alpha = 0$ for regular hexagrid, $\alpha = 1$ for the maximum irregularity. The relative density is defined as $\rho = V_g/V_d$, the ratio of the volume occupied by the grid $V_g = \sum_i l_i \cdot A_i$ (with l_i, A_i lengths and areas of the beams, respectively) to the solid volume of the entire tube or design space $V_d = 4L \cdot H \cdot b$ (with $L = 53\,m$ building side, $H = 391\,m$

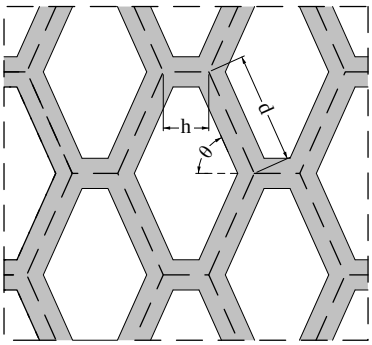

FIGURE 9 Reference hexagrid to initiate the stiffness-based design.

height, and b tube width, which is supposed to be equal to the width of the grid cross-section).

In the present work, the Vorogrids are obtained geometrically as in sec. 4.2 from different numbers of seed samples with the objective to score a similar overall total length $\sum_i l_i$, and therefore a similar relative density ρ because the cross-section is constant (tab. 1). Since the differences among the cases are not considered, a unique ρ is input as the mean density. The parameter α is taken as 0.8 from a visual comparison of the Vorogrid patterns with the design solutions proposed by Mele et al. (2019).

Unlike Mele et al. (2019), the Vorogrid meshes are not an outcome of altering an hexagrid. However, fixing a reference hexagonal cell is required to initialize the homogenization procedure. The adopted cell is found by tessellating a tube face with all-equal hexagons to have a similar number of seeds to the Vorogrids (816). The resulting hexagon is shown in fig. 9 and has $h = 1.66\ m$, $d = 4.05\ m$, $\theta = 65.85°$. Then, cross-section values are input, so the actual densities can be updated for both the Vorogrid (A_i constant term) and the homogenized tube (b term). The definition of reference hexagrid and the cross-section leads to the computation of the correction factors on a statistical basis from the ratios of moduli of the Voronoi over the reference hexagrid (both in axial and shear directions). The cross-section is updated until a target top deflection of $\Delta = H/500 = 0.702\ m$ is reached. In the present case, a Square Hollow Section (SHS) tube of $1.10 \times 1.10\ m$ with thickness $s = 0.09\ m$, corresponding to the correction factors $\eta_{E1} = 0.9724$, $\eta_{E2} = 1.0422$, $\eta_{G12} = 1.0282$, scores exactly $\Delta = 0.702\ m$. At this stage, the Vorogrid is supposed to bear the entire wind loading, so the cross-section is overestimated in terms of stiffness.

It is worth mentioning that this preliminary design should be subordinated to the geometry selection of the grid and not only to a density value ρ. Indeed, this latter parameter appears not descriptive enough as shown in fig. 10 because Vorogrids with the same density ρ behave differently. Nonetheless, the actual deformation of the patterns is below the $H/500$ target, and so the cross-section can be deemed oversized for the tested cases. The scattering of data remains for Vorogrids with different mesh and density, even though case-dependent trends can be highlighted.

The value of this preliminary design is twofold. First, it concludes that state-of-the-art methods could be applied to Vorogrids, although the result is affected by a certain deviation. Second, it returns a tentative cross-section, which constitutes the base for further refining as in sec. 4.5, also considering the core's contribution in providing lateral stiffness and the effect of vertical load.

TABLE 1 Statistics of the Voronoi patterns for all examined cases.

Case	Length (m)	Num. seeds n	Density ρ
(a)	0.01 - 7.07	783	0.127
(b)	0.21 - 9.99	766	0.121
(c)	0.05 - 12.17	838	0.122
(d)	0.12 - 12.79	745	0.121
(e)	0.03 - 9.86	708	0.121
(f)	0.03 - 12.44	714	0.121
Mean	3.18	759	0.121

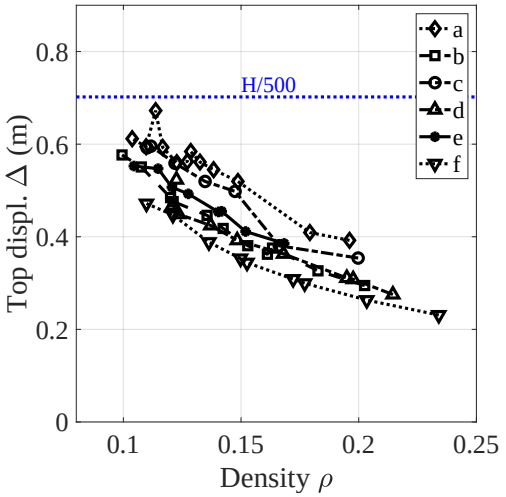

FIGURE 10 Sensitivity analysis of the density parameter ρ for a fixed Vorogrid cross-section SHS $1.10 \times 1.10\ m$, $s = 0.09\ m$, computed from a 3D model without core under lateral load only (in a linear simulation).

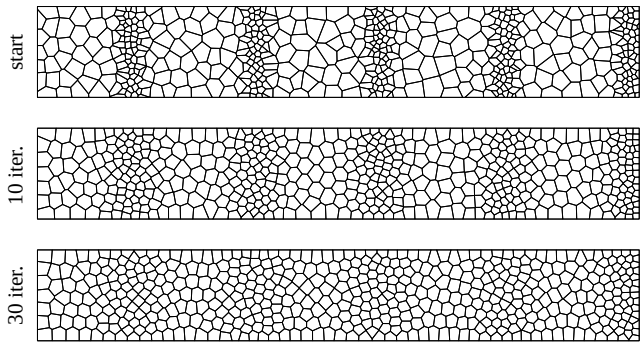

FIGURE 11 Lloyd relaxation of a Voronoi diagram derived from a random distribution of seeds.

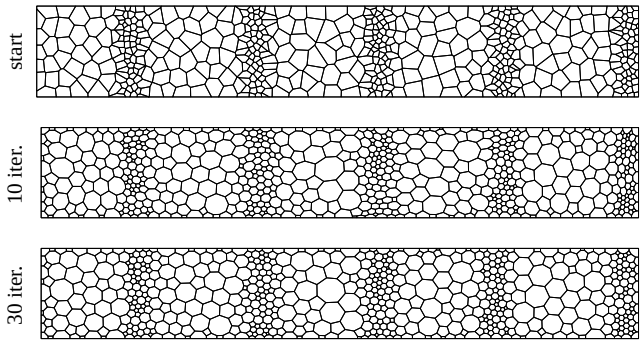

FIGURE 12 Driving the dual triangle mesh to a CP mesh, given a Voronoi diagram derived from a random distribution of seeds.

4.4 | Vorogrid optimization

4.4.1 | Geometric optimization

The reason for addressing geometric optimization lies on the necessity to avoid mesh degeneration in the form of sharp angles and short edges. On the one hand, these can turn into structural inefficiency, i.e. stress peaks may be produced if the grid is abruptly distorted or if some elements are locally too stiff. On the other hand, these can develop construction issues, i.e. complex and large nodes or unfeasible details. On this latter point, it should be considered, for instance, that several conflicts may be produced since Voronoi edges as beams are provided with proper width and merge with variable angles.

A global optimization that improves the shape of Voronoi cells can be performed through the Lloyd relaxation algorithm. The algorithm iterates over the positions of the seeds and moves them to generate increasingly accurate approximations of a centroidal Voronoi tessellation of the input, as shown in fig. 11 .

Given a Voronoi mesh and its triangular dual, the more the center of the circumcircle of a triangle is far from its barycenter, the less regular will be the Voronoi cell. Therefore, another global optimization alternative to foster the regularity of Voronoi cells is to push the dual triangular mesh to be a CP mesh (Schiftner, Höbinger, Wallner, & Pottmann, 2009), namely a triangulation where the inscribed circles of two adjacent triangles have a contact point on the shared edge, as shown in fig. 12 . A drawback of both methods, if lead to convergence (or performing a high number of iterations), is the loss of information about seeds' densities and the tendency to conform and regularize the cells (last row of figs.11 -12). However, the Vorogrid pipeline adopts the CP mesh optimization strategy up to 10 iterations because it balances geometric improvements while preserving the grid features.

Other actions can be performed at the local level to improve both the mesh quality and the subsequent structural behavior (fig. 13), such as:

- vertex collapse, which aims at merging pairs of vertices that are too close, this work considers the beam width as the limit distance for vertex collapse;
- vertex snap to other structural elements, which aims at moving the Voronoi vertices on the slabs or on the edge beams of the building to avoid short elements and closer nodes.

The effect of these local modifications on beam lengths are shown in fig. 14 . In the Vorogrid pipeline, both local strategies are adopted.

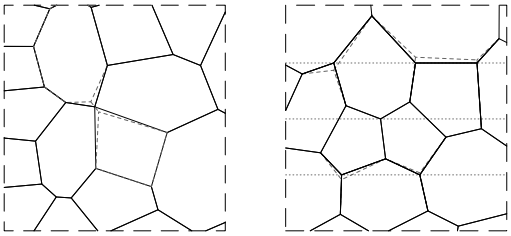

FIGURE 13 Local improvements (edited cells are dashed): on the left, vertex collapse; on the right, vertex snap to slabs (dotted lines).

4.4.2 | Structural optimization

A major issue of Voronoi meshes used as structures lies in the stress concentrations that occurs due to the grid's randomness with respect to the loading direction. The stress on a Voronoi cell is not only function of its size and shape but also depends on it neighboring cells. The total stress can be minimized while

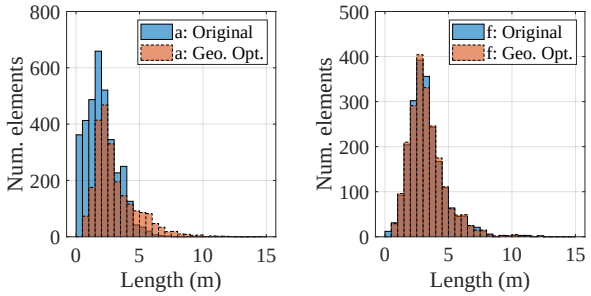

FIGURE 14 Histogram of the lengths' distribution in the original mesh and after both improvements of vertex collapse and vertex snap to slabs: on the left, case (a); on the right, case (f).

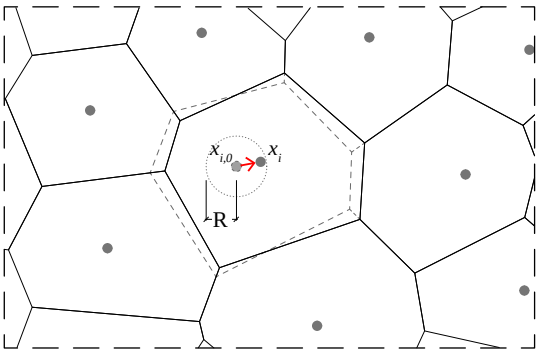

FIGURE 15 Schematics of the optimization problem in which the seeds of the most stressed Voronoi cell are moved within a circular neighboring of radius R.

satisfying the global equilibrium by moving the seeds in a circular domain, as shown in fig. 15 .

This optimization problem can be thus formulated as the following.

$$min\ \sigma(x_i) \tag{1}$$

$$\text{subject to:} \quad K(x_i) \cdot u = F \tag{2}$$

$$(x_i - x_{i,0})^2 \leq R_i^2 \tag{3}$$

where x_i is the vector of variables, namely the current positions of the n Voronoi seeds, $x_{i,0}$ is their starting position, σ is the maximum stress computed on each beam, R_i is the radius of the circular domain of the variable centered in $x_{i,0}$. Eq. 2 expresses the equilibrium condition according to the displacement method, in which $K(x_i)$ is the stiffness matrix, u is the vector of unknowns, namely the nodes displacements, and F is the vector of external forces. Considering the different sizes of Voronoi cells, the domain of the variables is supposed to be size-dependent not distorting the initial geometry. Therefore, for each step and for each Voronoi cell the radius is bounded by $R_i = c \cdot \sqrt{A_i/\pi}$, where A_i is the area of the i-th cell and c is a reduction factor equals to 0.5 in the current case.

Eqs. 1-3 describe a constrained nonlinear optimization problem that can be solved using several state-of-the-art algorithms. Among them, good performances have been obtained with the derivative-free Subplex algorithm implemented in the grasshopper plug-in goat (Rechenraum GmbH, 2021), using as termination criterion a maximum of 10k evaluations of the static solution.

The optimization has been performed using Karamba3D (Preisinger & Heimrath, 2014) as FEM solver and, to limit the computational job, it has been restricted to only a single face of the building, which is supposed to be loaded at the SLS with its tributary vertical load and half of the entire wind loading. In the current implementation, the stress σ is replaced by the utilization factor U, which expresses the beam's demand over capacity ratio according to the Eurocode 3 verification formulae within Karamba3D.

This optimization shows an expected load-dependency due to the randomness of the grid, so the selection of the vector of forces F is not trivial. First, concerning lateral loads, the output is influenced by the wind load direction. To consider this effect both wind directions are included as different load cases, and the beam utilization factor is evaluated as the maximum out of the two. Second, adding the vertical load alters the stress paths and lead to different optimized Vorogrids configurations. But concurrently, the exact amount of vertical load can not be known in this phase because it depends on the relative stiffness of the grid with respect to both the core. Therefore, the vertical load computed for the tributary slab area is added to the previous load cases in a SLS load combination. This limitation can be overcome if the problem is solved in a 3D setup, in which the correct spatial distribution of loads and load-bearing elements is better captured, but a far more intensive computational power is needed.

As reported in Fig. 16 , the resulting histogram after the optimization confirms the element utilization under SLS lateral load only and SLS combined lateral and vertical load, respectively. The combined load remarkably triggers higher stress throughout the grid, so it appears more reasonable to perform the optimization in this case since it would be closer to the real behavior. These latter results are used in the final 3D examples included in Sec. 5.

The restraints between the Vorogrid and the slabs are included in the optimization routine as provided by rigid weightless beams. Concurrently, the grid elements that intersect the slabs are segmented, creating an additional structural node. This procedure overloads beam segments that are too small. However, as mitigation to this problem, the vertex snap strategy is applied at each optimization step.

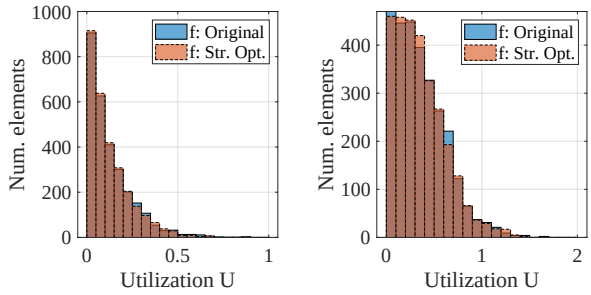

FIGURE 16 Histogram of the beams' utilization U in the original mesh and after the structural optimization of eqs. 1-3 for the case f: on the left, lateral wind loading; on the right, combined lateral and vertical loading.

Globally, the structural optimization output demonstrates the validity of the proposed approach even considering different load cases. Starting from the original mesh, a sensible stress reduction is obtained in all cases as highlighted in tab. 2 . Overall, this result leads also to a reduction of the mean and average values, meaning that the optimization thus formulated alters the whole statics of the grid positively. It is worth noticing that the loads are overestimated in this planar case, so it might happen that even after the optimization the peak values result far beyond the material capacity ($U \geq 1$, as for the combined load case). On a qualitative basis, the optimization shows a local character, namely the seeds' alterations are small and unable to deform the mesh design prominently.

4.5 | 3D model and sizing refinement

For each structural scheme of fig. 2 , a 3D model is built by replicating the Vorogrid face after the optimization by symmetry about the plan diagonals. The aim is (a) to assess the effectiveness of the proposed pipeline and (b) to size the grid. It is recommended for the edges that merge on the corners, from different sides of the building, to have coincident nodes for the sake of reducing shear and bending. This requirement is implicitly fulfilled by adopting the current mapping scheme. Moving from 2D to 3D the model is enriched with the core, the slabs, and more accurate restraints.

The FE model is linked to the parametric geometric model and is automatically analyzed in SAP2000 (Computers and Structures, Inc., 2021). The Vorogrid consists of a beam network that is fixed on the ground and is attached to each slab. The slabs are thick shells spanning from the tube to the core, which distribute the tributary lateral and vertical loads as defined in sec. 4.1. The core is modeled through shell elements. The gravity loads on the structural members are deduced from their section properties. Wind load is lumped and applied to each slab. All other loads are uniformly distributed on the slabs. All analyses consider nonlinear geometry effects and the EC load combinations of Tab. 3 at the ULS with maximum effect and at the SLS to assess internal forces and displacements, respectively.

Once the 3D model is created, the strength and stiffness can be tuned along the height of the building, solving a sizing problem. Since the design domain is the Vorogrid, only the cross-sections of its members are modified without altering the geometry and the remaining parts of the building. To keep the problem tractable, clusters of grid members can be defined by their positioning in height, and for each cluster a uniform cross-section can be plugged in.

For the present cases, the building is divided into five stacking modules of beams. Then, found a discrete set of standard cross-section sizes, the current cross-section properties of the clusters initially set as per Sec. 4.3 are updated manually by tapering until the requirements are met.

5 | RESULTS AND DISCUSSION

This section includes the results of 3D structural analyses and the discussion on six case studies in comparison with state-of-the-art solutions. The Vorogrids are obtained from the pipeline of fig. 1 , which streams selected strategies for the grid processing. For the grid initialization the remesh-from-distance approach is used on all schemes (previously shown in fig.2). This approach has been preferred for its consistency and for the aesthetic quality of the resulting mesh. All Vorogrids have been submitted to geometric and structural optimization under the SLS combination of vertical and lateral loads.

For the experiments to be comparable, the adopted equivalence criterion for the tube structures is they have approximately the same dead load, which is the same of having a similar total length of the mesh edges. This criterion inherently applies since the mesh generation step because the objective was to obtain an almost-constant density ρ. Moreover, it applies also when comparing Vorogrids with state-of-the-art solutions, such as diagrid (dia), hexagrid (hex) and random Voronoi (rVo, Fig. 17). Some statistics of the case studies are reported in tab. 4 . Diagrids are remarkably advantageous for a similar total length because they have fewer and all-equal beams and nodes. However, their hidden cost lies in the node technical complexity, having 6 beams merging per node. Conversely, all other poly-grid cases benefit from a low connectivity (3 beams per node). However, all nodes and all beams are different from each other.

TABLE 2 Stress reduction after the structural optimization of eqs. 1-3 for all examined cases (U values are EC3-compliant beams utilization factors).

Load Case	Case	U_{start}			U_{end}			$\Delta max(U)$	$\Delta max(U)$
		max()	mean()	median()	max()	mean()	median()		(%)
SLS Wind only	(a)	1.485	0.101	0.056	1.019	0.101	0.056	0.466	31.4
	(b)	0.953	0.119	0.076	0.684	0.117	0.077	0.269	28.3
	(c)	0.829	0.118	0.073	0.750	0.077	0.269	0.079	9.6
	(d)	1.028	0.101	0.055	0.946	0.073	0.079	0.082	8.0
	(e)	0.872	0.118	0.071	0.706	0.056	0.082	0.166	19.0
	(f)	0.888	0.129	0.091	0.658	0.124	0.090	0.230	25.8
SLS	(a)	7.320	0.333	0.220	1.950	0.307	0.217	5.370	73.4
	(b)	2.610	0.346	0.274	1.559	0.344	0.274	1.052	40.3
	(c)	1.643	0.355	0.270	1.548	0.346	0.272	0.095	5.8
	(d)	4.022	0.322	0.242	1.791	0.318	0.241	2.231	55.5
	(e)	3.480	0.348	0.272	1.576	0.345	0.271	1.904	54.7
	(f)	1.877	0.367	0.316	1.452	0.360	0.315	0.426	22.7

TABLE 3 Coefficients applied to characteristics loads for the adopted ULS and SLS load combinations (loads are structural G_1, non-structural G_2, variable Q_k, wind Q_w).

Name	G_1	G_2	Q_k	Q_w
ULS1	1.30	1.30	1.50	0.00
ULS2	1.00	1.00	0.00	1.50
ULS3	1.30	1.30	1.50	0.90
SLS1	1.00	1.00	0.70	1.00

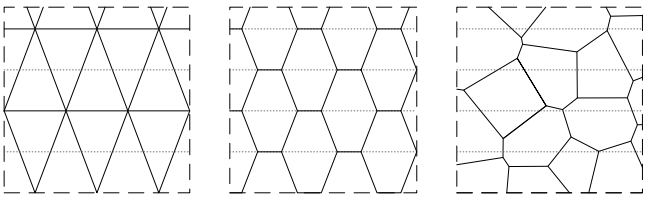

FIGURE 17 Adopted state-of-the-art tessellations having similar total beam length, from left: diagrid (dia), hexagrid (hex), random Voronoi (rVo).

TABLE 4 Vorogrid statistics for all examined 3D models

Case	**Beams**	**Nodes**	**Length** (m)	**Tot. length** (m)
(a)	10940	8144	0.50 - 10.0	26751
(b)	10478	7586	0.51 - 9.3	26833
(c)	10246	7614	0.51 - 8.5	26652
(d)	10404	7732	0.50 - 8.5	26734
(e)	9770	7170	0.51 - 9.2	26968
(f)	10262	7574	0.50 - 8.5	26764
(dia)	3240	1656	4.17 - 5.9	27012
(hex)	7772	5280	2.27 - 4.2	26873
(rVo)	6694	4338	0.42 - 9.7	26164

5.1 | Performance assessment and comparison with state-of-the-art patterns

Fig. 18 reports the SLS displacement of all models having a same uniform cross-section of $1.10 \times 1.10\ m$, $s = 0.09\ m$. As expected, the (dia) outperforms all other cases concerning stiffness, while all other Voronoi-based examples are in agreement, including the (rVo). The (hex) has an intermediate behavior.

In terms of absolute displacements, the best Vorogrid solutions are models (f), (b), (e) and (c), which are inspired by stress lines and mega frame schemes (mega columns, braced frame and mega frame). On the one hand, this result confirms that it is worth altering Voronoi meshes using statics-driven approaches (as in Pietroni et al. (2015)), since stress inspired meshes obtained with the Vorogrid method have good stiffness. On the other hand, it seems that this result is aligned with mega frames feature of being ideal structural systems for super tall buildings, as they can provide high lateral rigidity for a minimum weight. Therefore, in terms of stiffness, designing a frame-inspired Vorogrid is a valuable strategy as the method can inherit this feature from the initial structural schemes. The stiffness of model (f) shall be additionally improved if, instead of mapping the same grid (obtained from planar cantilever stress lines) on all building faces, the tube stress lines (similarly

to Cascone et al. (2021)) are considered and jointly optimized. The other models (a) and (d) performances are worse than the (rVo). The main factor affecting them is the less-dense grid in corner areas if compared to other Vorogrids.

In terms of interstory drift, a similar trend can be observed: the (dia) is still outperforming with respect to the (hex) and to the cluster of all other cases. The randomness of the tessellation is a characteristic of all Voronoi-based models and can lead to fluctuating values. This issue is to be considered in the detailed design phase as it may require a wider displacement capacity for the secondary elements.

All deformed configurations indicate a bending behavior with a stiffening effect in the upper third of the elevation, which shows a more linear deformation in the absolute displacement and an almost-constant interstory drift. The bending-type deformed shape in the fist two thirds of the building is mostly imposed by the core. If the core is removed, the deformed shapes are more linear. The extreme cases are: model (a), having the most linear behavior, and model (d), in which the deformed shapes with- and without-core are closer. Model (f) has similar features to (d). The stiffening effect is due to the use of a constant beams' cross-section and is attenuated if refined. Moreover, in some case, the stiffening effect is larger because more small and rigid cells are located in the upper part (i.e. models (a), (c), (d)). In general, considering the variety of Vorogrids the displacement variation is included in a narrow spectrum of values. The narrowing occurs as an outcome of geometric and structural optimization.

All models show absolute and relative displacements that are well within the common limitations $\Delta < H/500 = 0.702\,m$ and $\delta_i < h/300 = 0.013\,m$ respectively. This outcome is also a byproduct of using a non-tapered stiff core. Although it may seem redundant, such a core is strictly necessary from the strength point of view for guaranteeing ULS performances for the Vorogrids, especially at the lowest levels.

Fig. 19 plots the von Mises stress for the grid elements under the most demanding load combination ULS3. The per-element stress of Vorogrids is in many cases beyond the material resistance, unlike (dia) and (hex) where the demand over capacity ratio is lower than 0.7. For this reason, the cross-section of Vorogrids require a strength refinement. Indeed, even if well calibrated from the stiffness point of view (see previous Fig. 10), the cross-section determined as in Sec. 4.3 must be intended as an initialization value. The cross-sections are modified using five clusters of members as shown in Fig. 20 iteratively until the desired strength is reached, once the core is added and all load combinations are considered.

The point scattering arising in both charts of Fig. 19 (regardless of using constant or refined cross-sections) denotes a large spectrum of element utilization. If on the one hand it leads to the exploitation of the entire range of strength capacity

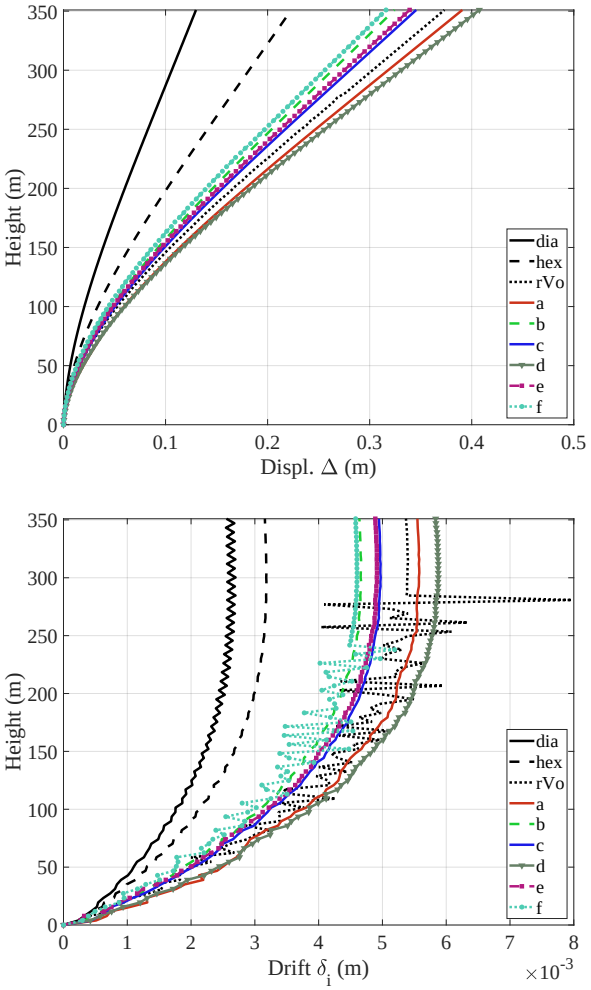

FIGURE 18 SLS absolute displacement and interstorey drift.

and to the possibility of achieving robustness, on the other hand it constitutes an actual barrier to adopting a finer clustering of members in which the cross-section is not oversized. Concerning state-of-the-art solutions, (dia) and (hex) models do not suffer from strength problems (Fig. 19) since, as well known, their design is governed by stiffness. Indeed, their cross-section could be rather reduced for material saving. Instead, the (rVo) model (omitted from the figure) has a bending-dominated grid that makes it akin to Vorogrid structures. And similarly the stiffness based criterion can only provide a tentative section to be later refined.

In general, Voronoi-based patterns can hardly be used if not in combination with a core. Alternatively, a high-strength material could be used. Indeed, this work employed S275 steel to effectively compare the Vorogrids with other competitors and previous research data, but choosing a high-strength material would result in a more balanced design between stiffness and strength.

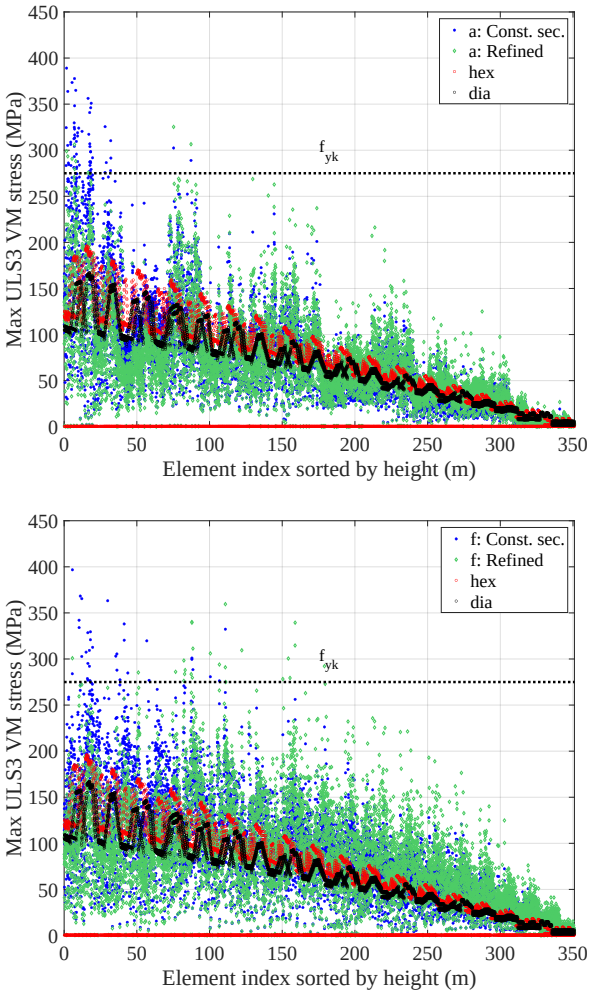

FIGURE 19 ULS3 strength verification before and after the refinement for the cases (a) and (f) in comparison with (dia) and (hex).

After the section refinement, in the experiments there are still a few beams stressed beyond the material threshold. In this case, it is not appropriate to assign a larger section to the whole cluster because the provided benefits would be small if compared to the added load. Instead, this demand could be better satisfied locally by altering the section where needed.

It is interesting to observe other features of Vorogrids from their macroscopic behavior. Fig. 21 reports on the cumulative interior forces in the worst load combinations (the cross-section is constant). Cases (a) and (d) behave similarly to tall buildings with outriggers that they mimic: the axial and shear forces have an oscillating trend around the outrigger areas where the Vorogrid is denser and stiff as the core; and the bending plot of the core apart from small fluctuations appears

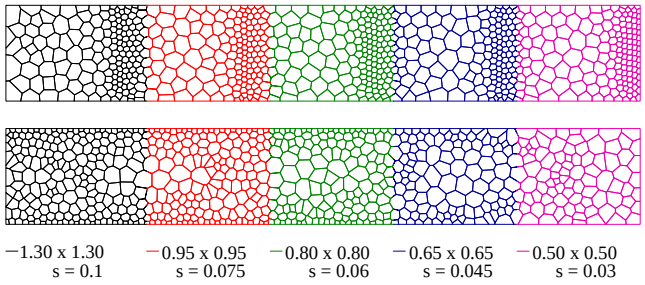

FIGURE 20 Members' cross-section refinement: top, case (a); bottom, case (f).

similar to an outrigger-supported core, in which the grid performs as an exterior plate in tension-compression and relieves the core. In these cases, the grid reaches a high strength ratio.

Due to the higher density around the corners, the case (b) shows the highest bending strength, but it seems to be more sensitive to the shear lag effect. Case (c) is a combination of the features of (a) and (b). In the case (e), the horizontal attractor lines of the braced tube increase locally the stiffness of the grid, which shows signs of a belt truss behavior. This effect characterizes positively the bending force on the core which is lower than in previous cases, except for local peaks. The case (f), similarly to (b), makes maximum use of the external tube in supporting loads. Interior forces flow at an almost-constant ratio throughout the building.

Overall, as tube structures, a common characteristic of Vorogrids is the high bending strength. Conversely, shear and axial forces are carried more by the core. This latter effect is typical of generic random Voronoi buildings, but it is not observed in the (dia) and (hex) cases, where the contribution of the grid is always prevalent since they bear vertical and shear loads more efficiently. In particular, shear resisting mechanism is the key of success of diagrid, and a more slender core shall be used in diagrids and hexagrids. The advantage of these systems constitutes the main lack of Vorogrids (and similarly of random Voronoi), which are not able to mobilize axial-prevailing member forces because of the geometry of the pattern. In fact, by observing in detail the grid behavior it appears clear that its structural response combines all kinds of internal forces. Fig. 22 reports the diagrams of the axial force and bending moment for two exemplary cases (b) and (f) at the most stressed areas of the building. The maximum per-section von Mises stress spreads over the whole grid, however, it is caused also by bending moments, which affect only the extremes of the beams.

The same 3D models are used to run the natural frequency analysis of all examined Vorogrids. In addition to the structural elements' mass, the non-structural components on the slabs are

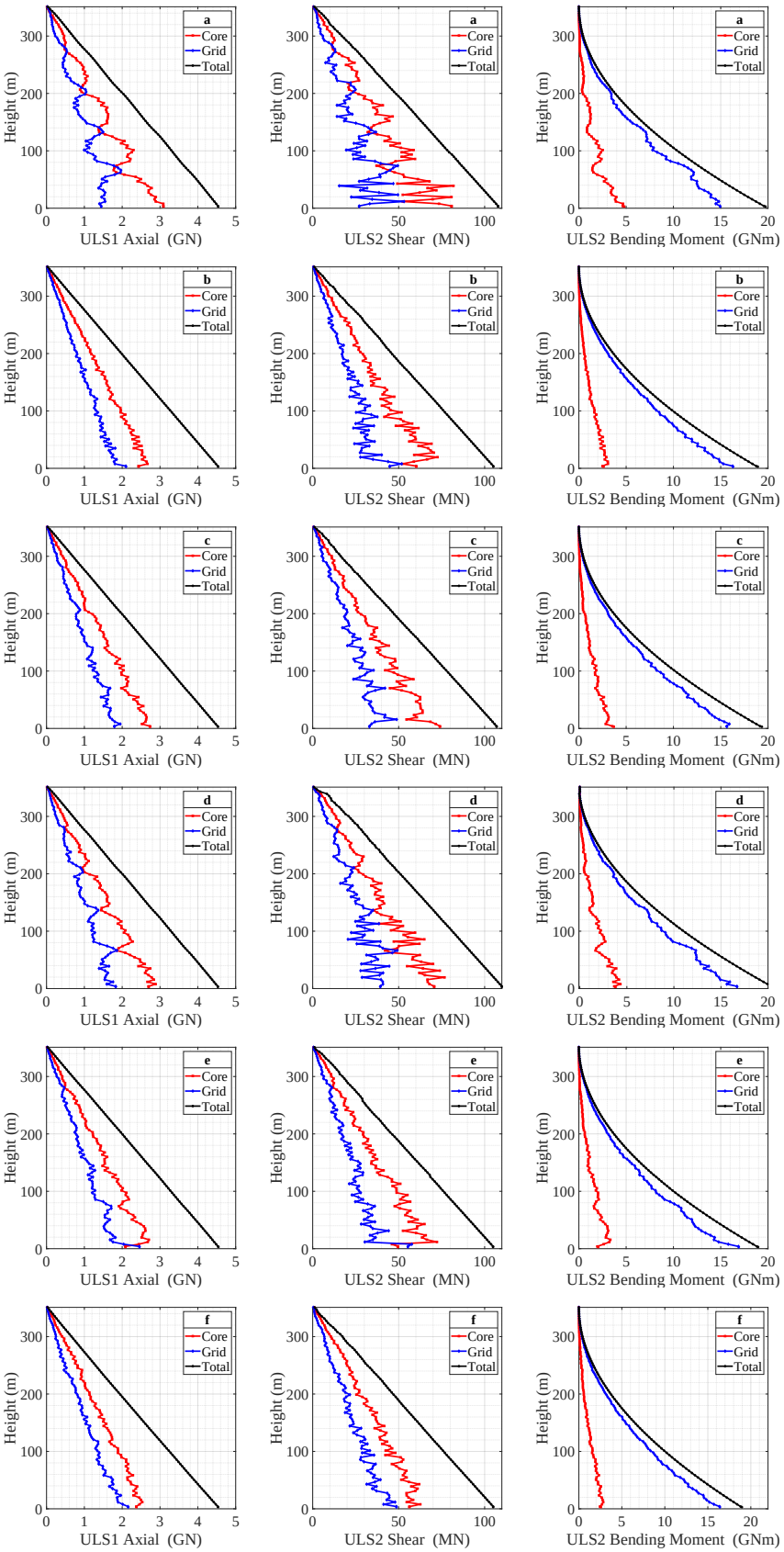

FIGURE 21 Interior forces, from the first row: cases (a); (b); (c); (d); (e); (f).

added as mass from the loads according to the EC combination $G_1 + G_2 + 0.3 \cdot Q_k$. Tab. 5 reports the first six periods and participating mass ratios for all cases. Fig. 23 shows the first six modal shapes for an exemplary case (d). With a small exception on models (b) and (e), all examples reveal a similar behavior. Modes 1 and 2 are translational modes in y and x directions, respectively. Mode 3 is the fundamental torsional mode. Mode 6 is the vertical mode along the z axis. The first six modes collect cumulative participating mass ratios higher than 80%, while 20 modes are sufficient to reach a modal participation higher than 90%. The first two modes of the cases (b) and (e) are not axis-aligned but instead are diagonal. Although the patterns are asymmetric with respect to the mid-faces axes, the natural frequency analysis exhibit symmetric mode shapes and mass participation (modes 1-2, and modes 4-5). More importantly, the dynamic stiffness of all cases is included in a narrow span: the first fundamental period ranges from 4.266 s of (c) to 4.678 s of (e). The state-of-the-art competitors show similar modes and modal participation, but a different dynamic stiffness: 4.049 s for (dia), 4.357 s for (hex), 4.752 s for (rVo), as first periods.

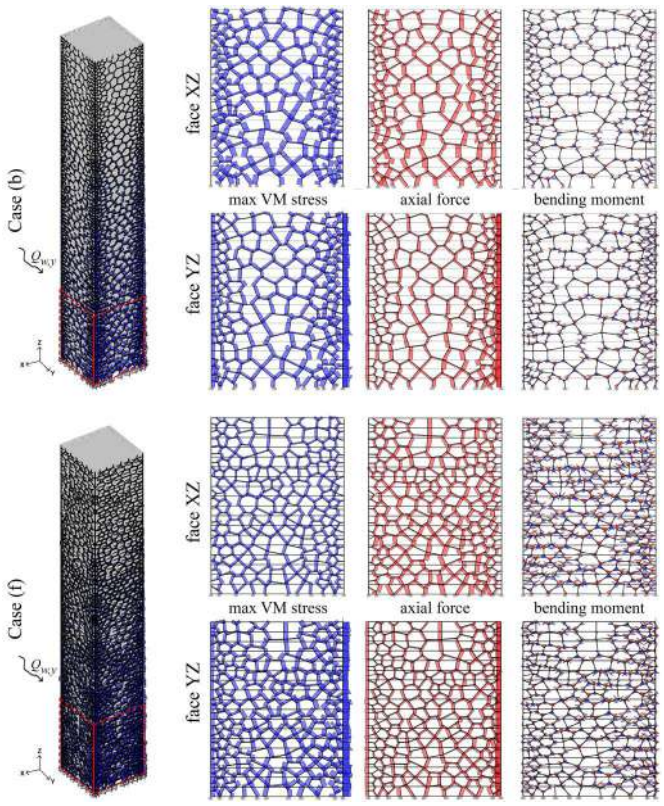

FIGURE 22 Structural behavior of the cases (b) and (f): maximum von Mises stress, axial force and bending moment distribution at the ULS3 for (part of) the downwind and lateral faces.

5.2 | Details and feasibility

A fundamental aspect of real world applications is fabrication. Obviously, the modular systems of diagrid and hexagrid have a matchless degree of prefabrication, and especially in presence of symmetry they can attain excellent cost-effectiveness. The premise of this work to find a pleasant-looking organic pattern is inherently combined with geometric complexity, which consequently leads to custom elements everywhere. Evidently, there is no room for comparison if standard techniques are used, instead this complexity can be advantageously managed by means of digital fabrication means in which the material/labor saving comes from the repetition of same manufacturing actions performed by numerically-controlled machines. However, even in absolute terms, some features positively affect the feasibility of Vorogrids. First, concerning fabrication, the adoption of a single cross-section for all members in a cluster may lead to a remarkable economy (if the material cost is not the main issue). Second, the use of three-way nodes is advantageous in terms of production, and in the authors' opinion they may present a potential that is still unlocked (especially from the mechanical point of view, i.e. damping capacity and robustness). Finally, in the current application case, the symmetry of the building about the orthogonal directions could be exploited to adopt a strictly symmetric Voronoi mesh, which have the advantage of increasing the prefabrication and obtain a more symmetric structural response.

6 | CONCLUSIONS

This paper introduced Vorogrid, a novel strategy to design Voronoi tube patterns for tall buildings, whose density is driven by lines and areas drawn on the surface and inspired by known structural schemes. The resulting structures have an organic and aesthetically-pleasant appearance, and show mechanical soundness. Overall, the most interesting feature offered by Vorogrid structures is their ability to reproduce some mechanical features of the schemes they mimic, such as the excellent rigidity for frame-inspired grids and the interior force distribution for outrigger-inspired grids. The structural response is uniquely function of the beams' distribution on the tube faces and suggests the substantial importance of the pattern on global performances. Therefore, the design intent of hiding a specific structural behavior behind an apparently-organic pattern is achieved.

All tested configurations show a high bending stiffness. However, unlike other discrete tubes, adopting an irregular polygonal pattern turned Vorogrids' structural behavior to be bending dominated. Thus, as opposed to diagrids, in which the grid is mainly engaged in axial stress and the shear resisting

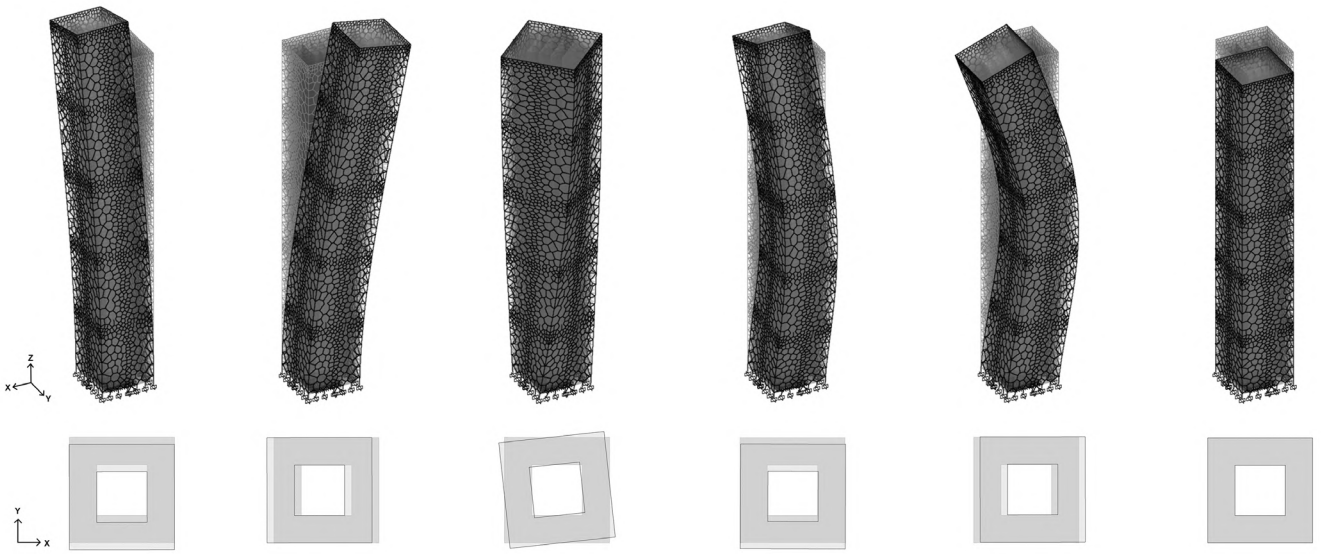

FIGURE 23 Natural frequency analysis: first six modal shapes for the case (d).

mechanism is effective, they undergo a complex and unevenly-efficient state of stress. Thus, diagrids remain outperforming in terms of stiffness and strength, but are based on a diamond pattern in use since 20 years. Concerning poly-meshes, Vorogrids can be located between hexagrids, which have better mechanical performances and regular tessellation, and random Voronoi structures, which are more chaotic in geometry and mechanics.

The bending-dominated random grid also highlighted another difference concerning state-of-the-art competitors: the design problem of Vorogrids is strength-based. So, even though stiffness-based methods used for random Voronoi patterns proved accuracy to some extent, the use of a core is recommended since the building would meet the displacement demands but overcome the material capacity. This remarkable behavior is shared by all Voronoi-based cases, including random Voronoi buildings. Questions remain about the ability of the current stiffness-based preliminary design to provide good initialization values for the cross-section. On the other hand, the irregularity and density variability of Vorogrids make a strength-based preliminary design hard to perform. Moreover, the core further complicates it. These have been the reasons why, as the last step, the cross-section is refined to fulfill strength requirements. Besides these aspects, all proposed Vorogrid examples excel in stiffness, having a low top and inter-story drift.

The presented method automated all the design steps that start from the structural schemes and lead to a 3D model of the building with its finite element representation. Moreover, it integrated structural and geometric optimization of the cells that mitigate localized peaks of stress caused by the randomness of Voronoi cells without sacrificing the organic appearance of the patterns. However, the computational power required by some operations was a drawback. So, they were conveniently performed in 2D, exploiting the symmetry of the building. However, a future 3D extension is recommended for accuracy and generality.

The novelty of the work is in the ability to control and improve the Voronoi scheme and make it suitable as a tube structure. The conceptual method proposed in this paper constitutes a design tool that expands the design possibilities for tall patterned buildings and supports the generation of potentially endless pattern design variations and solutions. The work characterizes the response of the main parameters to the overall structural behavior. Moreover, it makes a further step in applying and understanding how variable-shaped polygonal patterns could possibly be used as tube structures.

CONFLICT OF INTEREST

The authors declare no potential conflict of interests.

References

Adeli, H., & Cheng, N.-T. (1994). Concurrent genetic algorithms for optimization of large structures. *Journal of Aerospace Engineering*, *7*(3), 276–296. doi:

Adeli, H., & Kumar, S. (1995). Concurrent structural optimization on massively parallel supercomputer. *Journal of Structural Engineering*, *121*(11), 1588–1597. doi:

Adeli, H., & Park, H. S. (1995). Optimization of space structures by neural dynamics. *Neural networks*, *8*(5), 769–781.

TABLE 5 Natural frequency analysis: periods and participating mass ratios (x, y, z, r_x, r_y, r_z are translations and rotations in the global reference system as in Fig. 23).

Mode	Period	Participating Mass Ratios					
	(s)	x	y	z	r_x	r_y	r_z
			Case (a)				
1	4.568	0.06	0.56	0.00	0.33	0.04	0.00
2	4.362	0.57	0.06	0.00	0.04	0.33	0.00
3	1.329	0.00	0.00	0.00	0.00	0.00	0.84
4	1.149	0.10	0.11	0.00	0.13	0.11	0.00
5	1.142	0.11	0.10	0.00	0.11	0.13	0.00
6	0.592	0.00	0.00	0.82	0.00	0.00	0.00
			Case (b)				
1	4.331	0.28	0.33	0.00	0.20	0.17	0.00
2	4.205	0.33	0.28	0.00	0.17	0.20	0.00
3	1.275	0.00	0.00	0.00	0.00	0.00	0.81
4	1.084	0.08	0.12	0.00	0.13	0.09	0.00
5	1.077	0.12	0.08	0.00	0.09	0.13	0.00
6	0.582	0.00	0.00	0.81	0.00	0.00	0.00
			Case (c)				
1	4.266	0.51	0.11	0.00	0.07	0.31	0.00
2	4.142	0.11	0.51	0.00	0.31	0.07	0.00
3	1.262	0.00	0.00	0.00	0.00	0.00	0.81
4	1.101	0.08	0.12	0.00	0.14	0.09	0.00
5	1.092	0.13	0.08	0.00	0.09	0.14	0.00
6	0.584	0.00	0.00	0.81	0.00	0.00	0.00
			Case (d)				
1	4.502	0.62	0.01	0.00	0.00	0.36	0.00
2	4.235	0.01	0.63	0.00	0.36	0.00	0.00
3	1.284	0.00	0.00	0.00	0.00	0.00	0.82
4	1.138	0.20	0.00	0.00	0.00	0.23	0.00
5	1.136	0.00	0.19	0.00	0.24	0.00	0.00
6	0.589	0.00	0.00	0.82	0.00	0.00	0.00
			Case (e)				
1	4.678	0.34	0.27	0.00	0.17	0.21	0.00
2	4.531	0.27	0.34	0.00	0.21	0.17	0.00
3	1.278	0.00	0.00	0.00	0.00	0.00	0.81
4	1.100	0.08	0.13	0.00	0.14	0.08	0.00
5	1.096	0.13	0.08	0.00	0.08	0.13	0.00
6	0.583	0.00	0.00	0.81	0.00	0.00	0.00
			Case (f)				
1	4.580	0.03	0.58	0.00	0.37	0.02	0.00
2	4.202	0.58	0.03	0.00	0.02	0.37	0.00
3	1.212	0.00	0.00	0.00	0.00	0.00	0.80
4	1.074	0.00	0.20	0.00	0.21	0.00	0.00
5	1.067	0.20	0.00	0.00	0.00	0.20	0.00
6	0.570	0.00	0.00	0.81	0.00	0.00	0.00

doi:

Adeli, H., & Park, H. S. (1998). *Neurocomputing for Design Automation*. CRC Press, Inc.

Aldwaik, M., & Adeli, H. (2014). Advances in optimization of highrise building structures. *Structural and Multidisciplinary Optimization*, *50*(6), 899–919. doi:

Angelucci, G., & Mollaioli, F. (2017). Diagrid structural systems for tall buildings: changing pattern configuration through topological assessments. *The Structural Design of Tall and Special Buildings*, *26*(18), e1396. doi:

Angelucci, G., & Mollaioli, F. (2018). Voronoi-Like Grid Systems for Tall Buildings. *Frontiers in Built Environment*, *4*, 78. Retrieved from `https://www.frontiersin.org/article/10.3389/fbuil.2018.00078` doi:

Angelucci, G., Spence, S. M. J., & Mollaioli, F. (2020). An integrated topology optimization framework for three-dimensional domains using shell elements. *The Structural Design of Tall and Special Buildings*, e1817. Retrieved from `https://onlinelibrary.wiley.com/doi/abs/10.1002/tal.1817` doi:

Asadi, E., & Adeli, H. (2017). Diagrid: An innovative, sustainable, and efficient structural system. *The Structural Design of Tall and Special Buildings*, *26*(8), e1358. doi:

Asadi, E., & Adeli, H. (2018). Seismic performance factors for low-to mid-rise steel diagrid structural systems. *The Structural Design of Tall and Special Buildings*, *27*(15), e1505. doi:

Beghini, L. L., Beghini, A., Katz, N., Baker, W. F., & Paulino, G. H. (2014). Connecting architecture and engineering through structural topology optimization. *Engineering Structures*, *59*, 716 - 726. Retrieved from `http://www.sciencedirect.com/science/article/pii/S0141029613005014` doi:

Bruggi, M. (2020). Conceptual Design of Diagrids and Hexagrids by Distribution of Lattice Structures. *Frontiers in Built Environment*, *6*, 80. Retrieved from `https://www.frontiersin.org/article/10.3389/fbuil.2020.00080` doi:

Cascone, F., Faiella, D., Tomei, V., & Mele, E. (2021). Stress lines inspired structural patterns for tall buildings. *Engineering Structures*, *229*, 111546. Retrieved from `https://www.sciencedirect.com/science/article/pii/S014102962034147X` doi:

Computers and Structures, Inc. (2021). SAP2000 Structural Analysis and Design, Technical Knowledge Base. *Computer software documentation, https://wiki.csiamerica.com*.

Cucinotta, F., Raffaele, M., & Salmeri, F. (2019). A stress-based topology optimization method by a Voronoi tessellation Additive Manufacturing oriented. *The International Journal of Advanced Manufacturing Technology*,

103(5-8), 1965–1975. doi:

Fantini, M., & Curto, M. (2018). Interactive design and manufacturing of a Voronoi-based biomimetic bone scaffold for morphological characterization. *International Journal on Interactive Design and Manufacturing (IJIDeM)*, *12*(2), 585–596. Retrieved from https://doi.org/10.1007/s12008-017-0416-x doi:

Froli, M., & Laccone, F. (2017). Experimental static and dynamic tests on a large-scale free-form Voronoi grid shell mock-up in comparison with finite-element method results. *International Journal of Advanced Structural Engineering*, *9*(3), 293–308. doi:

Gunel, M. H., & Ilgin, H. E. (2007). A proposal for the classification of structural systems of tall buildings. *Building and environment*, *42*(7), 2667–2675. doi:

Gutierrez Soto, M., & Adeli, H. (2017). Many-objective control optimization of high-rise building structures using replicator dynamics and neural dynamics model. *Structural and Multidisciplinary Optimization*, *56*(6), 1521–1537. doi:

Hua, H., Hovestadt, L., & Tang, P. (2020). Optimization and prefabrication of timber Voronoi shells. *Structural and Multidisciplinary Optimization*, 1–15. doi:

Kim, H.-S., Lim, Y.-J., & Lee, H.-L. (2020). Optimum location of outrigger in tall buildings using finite element analysis and gradient-based optimization method. *Journal of Building Engineering*, *31*, 101379. Retrieved from https://www.sciencedirect.com/science/article/pii/S2352710219315827 doi:

Kociecki, M., & Adeli, H. (2014). Two-phase genetic algorithm for topology optimization of free-form steel space-frame roof structures with complex curvatures. *Engineering Applications of Artificial Intelligence*, *32*, 218–227. doi:

Kociecki, M., & Adeli, H. (2015). Shape optimization of free-form steel space-frame roof structures with complex geometries using evolutionary computing. *Engineering Applications of Artificial Intelligence*, *38*, 168–182. doi:

Laccone, F., Casali, A., Sodano, M., & Froli, M. (2021). Morphogenesis of a bundled tall building: Biomimetic, structural, and wind-energy design of a multi-core-outrigger system combined with diagrid. *The Structural Design of Tall and Special Buildings*, *30*(6), e1839. Retrieved from https://onlinelibrary.wiley.com/doi/abs/10.1002/tal.1839 e1839 tal.1839. doi:

Lacidogna, G., Scaramozzino, D., & Carpinteri, A. (2019). A matrix-based method for the structural analysis of diagrid systems. *Engineering Structures*, *193*, 340 - 352. Retrieved from http://www.sciencedirect.com/science/article/pii/S0141029618321953 doi:

Lee, S., & Tovar, A. (2014). Outrigger placement in tall buildings using topology optimization. *Engineering structures*, *74*, 122–129.

Li, S., Snaiki, R., & Wu, T. (2021). A knowledge-enhanced deep reinforcement learning-based shape optimizer for aerodynamic mitigation of wind-sensitive structures. *Computer-Aided Civil and Infrastructure Engineering*, *36*(6), 733-746. Retrieved from https://onlinelibrary.wiley.com/doi/abs/10.1111/mice.12655 doi:

Liu, B., Cao, W., Zhang, L., Jiang, K., & Lu, P. (2021). A design method of Voronoi porous structures with graded relative elasticity distribution for functionally gradient porous materials. *International Journal of Mechanics and Materials in Design*. Retrieved from https://doi.org/10.1007/s10999-021-09558-6 doi:

Liu, C., & Fang, D. (2020). Robustness analysis of vertical resistance to progressive collapse of diagrid structures in tall buildings. *The Structural Design of Tall and Special Buildings*, *29*(13), e1775. Retrieved from https://onlinelibrary.wiley.com/doi/abs/10.1002/tal.1775 e1775 TAL-19-0311.R1. doi:

Liu, C., Li, Q., Lu, Z., & Wu, H. (2018). A review of the diagrid structural system for tall buildings. *The Structural Design of Tall and Special Buildings*, *27*(4), e1445. Retrieved from https://onlinelibrary.wiley.com/doi/abs/10.1002/tal.1445 e1445 TAL-17-0073.R1. doi:

Mahjoubi, S., & Bao, Y. (2021). Game theory-based metaheuristics for structural design optimization. *Computer-Aided Civil and Infrastructure Engineering*, *36*(10), 1337–1353. doi:

Martínez, J., Dumas, J., & Lefebvre, S. (2016, July). Procedural Voronoi Foams for Additive Manufacturing. *ACM Trans. Graph.*, *35*(4). Retrieved from https://doi.org/10.1145/2897824.2925922 doi:

Martínez, J., Hornus, S., Song, H., & Lefebvre, S. (2018, July). Polyhedral Voronoi Diagrams for Additive Manufacturing. *ACM Trans. Graph.*, *37*(4). Retrieved from https://doi.org/10.1145/3197517.3201343 doi:

Mashhadiali, N., & Kheyroddin, A. (2013). Proposing the hexagrid system as a new structural system for tall buildings. *The Structural Design of Tall and Special Buildings*, *22*(17), 1310-1329. Retrieved from https://onlinelibrary.wiley.com/doi/abs/10.1002/tal.1009 doi:

McNeel, R., & Associates. (2020). Grasshopper generative modeling for Rhino. *Computer software, http://www.grasshopper3d. com*.

Mele, E., Fraldi, M., Montuori, G. M., Perrella, G., et al. (2019). Hexagrid-voronoi transition in structural patterns

for tall buildings. *Frattura ed Integrità Strutturale*, *13*(47), 186. doi:

Montuori, G. M., Fadda, M., Perrella, G., & Mele, E. (2015). Hexagrid-hexagonal tube structures for tall buildings: patterns, modeling, and design. *The Structural Design of Tall and Special Buildings*, *24*(15), 912–940. doi:

Montuori, G. M., Mele, E., Brandonisio, G., & De Luca, A. (2014). Design criteria for diagrid tall buildings: Stiffness versus strength. *The Structural Design of Tall and Special Buildings*, *23*(17), 1294–1314. doi:

Moon, K. S. (2008). Optimal Grid Geometry of Diagrid Structures for Tall Buildings. *Architectural Science Review*, *51*(3), 239-251. Retrieved from https://doi.org/10.3763/asre.2008.5129 doi:

Moon, K. S. (2010). Stiffness-based design methodology for steel braced tube structures: A sustainable approach. *Engineering Structures*, *32*(10), 3163-3170. Retrieved from https://www.sciencedirect.com/science/article/pii/S0141029610002440 doi:

Moon, K.-S., Connor, J. J., & Fernandez, J. E. (2007). Diagrid structural systems for tall buildings: characteristics and methodology for preliminary design. *The structural design of tall and special buildings*, *16*(2), 205–230. doi:

Oh, B. K., Glisic, B., Kim, Y., & Park, H. S. (2019). Convolutional neural network-based wind-induced response estimation model for tall buildings. *Computer-Aided Civil and Infrastructure Engineering*, *34*(10), 843-858. Retrieved from https://onlinelibrary.wiley.com/doi/abs/10.1111/mice.12476 doi:

Pietroni, N., Tonelli, D., Puppo, E., Froli, M., Scopigno, R., & Cignoni, P. (2015). Statics aware grid shells. *Computer Graphics Forum*, *34*(2), 627-641. Retrieved from https://onlinelibrary.wiley.com/doi/abs/10.1111/cgf.12590 doi:

Piker, D. (2013). Kangaroo: form finding with computational physics. *Architectural Design*, *83*(2), 136–137. doi:

Preisinger, C., & Heimrath, M. (2014). Karamba - A toolkit for parametric structural design. *Structural Engineering International*, *24*(2), 217–221. doi:

Rechenraum GmbH. (2021). goat® optimization solver component for Rhino's Grasshopper. *Computer software documentation, http://www.rechenraum.com/*.

Sarcheshmehpour, M., & Estekanchi, H. E. (2021). Life cycle cost optimization of earthquake-resistant steel framed tube tall buildings. *Structures*, *30*, 585-601. Retrieved from https://www.sciencedirect.com/science/article/pii/S2352012421000424 doi:

Sarcheshmehpour, M., Estekanchi, H. E., & Moosavian, H. (2020). Optimum seismic design of steel framed-tube and tube-in-tube tall buildings. *The Structural Design of Tall and Special Buildings*, *29*(14), e1782. Retrieved from https://onlinelibrary.wiley.com/doi/abs/10.1002/tal.1782 e1782 TAL-20-0006.R1. doi:

Sarma, K. C., & Adeli, H. (2001). Bilevel parallel genetic algorithms for optimization of large steel structures. *Computer-Aided Civil and Infrastructure Engineering*, *16*(5), 295–304. doi:

Sarma, K. C., & Adeli, H. (2003). Data parallel fuzzy genetic algorithm for cost optimization of large space steel structures. *International Journal of Space Structures*, *18*(3), 195–205.

Schiftner, A., Höbinger, M., Wallner, J., & Pottmann, H. (2009). Packing Circles and Spheres on Surfaces. In *Acm siggraph asia 2009 papers.* New York, NY, USA: Association for Computing Machinery. Retrieved from https://doi.org/10.1145/1661412.1618485 doi:

Su, Y., Wu, Y., Ji, W., & Sun, X. (2020). Computational morphogenesis of free-form grid structures with voronoi diagram. *Computer-Aided Civil and Infrastructure Engineering*, *n/a*(n/a). Retrieved from https://onlinelibrary.wiley.com/doi/abs/10.1111/mice.12621 doi:

Tomei, V., Imbimbo, M., & Mele, E. (2018). Optimization of structural patterns for tall buildings: The case of diagrid. *Engineering Structures*, *171*, 280–297. doi:

Tonelli, D., Pietroni, N., Puppo, E., Froli, M., Cignoni, P., Amendola, G., & Scopigno, R. (2016). Stability of Statics Aware Voronoi Grid-Shells. *Engineering Structures*, *116*, 70 - 82. Retrieved from http://www.sciencedirect.com/science/article/pii/S0141029616300074 doi:

Zhao, F., & Zhang, C. (2015). Diagonal arrangements of diagrid tube structures for preliminary design. *The Structural Design of Tall and Special Buildings*, *24*(3), 159-175. Retrieved from https://onlinelibrary.wiley.com/doi/abs/10.1002/tal.1159 doi:

Zhou, Z., Qian, J., Huang, W., & Yao, K. (2021). Seismic damage assessment of a supertall tubed mega frame structure based on a simplified finite element model. *The Structural Design of Tall and Special Buildings*, *30*(7), e1846. Retrieved from https://onlinelibrary.wiley.com/doi/abs/10.1002/tal.1846 doi:

□